Observation of very high order multi-photon absorption in GeSbS chalcogenide glass (EP)

Byoung-Uk Sohn (iD), Myungkoo Kang, Ju Won Choi (iD), Anuradha M. Agarwal (iD), Kathleen Richardson, and Dawn T. H. Tan (iD)

COLLECTIONS

EP   This paper was selected as an Editor's Pick

View Online   Export Citation   CrossMark

ARTICLES YOU MAY BE INTERESTED IN

Strong frequency conversion in heterogeneously integrated GaAs resonators
APL Photonics 4, 036103 (2019); https://doi.org/10.1063/1.5065533

Background-free time-resolved coherent Raman spectroscopy (CSRS and CARS):
Heterodyne detection of low-energy vibrations and identification of excited-state
contributions
APL Photonics 4, 056102 (2019); https://doi.org/10.1063/1.5090585

Cryptography in coherent optical information networks using dissipative metamaterial
gates
APL Photonics 4, 046102 (2019); https://doi.org/10.1063/1.5092216

Observation of very high order multi-photon absorption in GeSbS chalcogenide glass

View Online   Export Citation   CrossMark

Byoung-Uk Sohn,[1] (ID) Myungkoo Kang,[2] Ju Won Choi,[1] (ID) Anuradha M. Agarwal,[3] (ID) Kathleen Richardson,[2] and Dawn T. H. Tan[1,a] (ID)

AFFILIATIONS

[1] Photonics Devices and System Group, Engineering Product Development, Singapore University of Technology and Design, Singapore 487372, Singapore
[2] College of Optics and Photonics, University of Central Florida, Orlando, Florida 32816, USA
[3] Materials Research Laboratory, Massachusetts Institute of Technology, Cambridge, Massachusetts 02139, USA

[a] Author to whom correspondence should be addressed: dawn_tan@sutd.edu.sg

ABSTRACT

We report high order multi-photon absorption in $Ge_{23}Sb_7S_{70}$ chalcogenide glasses up to the 11th order. Open aperture z-scan measurements with enhanced detection capabilities are performed at short-wave to mid-infrared wavelengths between 1.1 μm and 5.5 μm, enabling very high order multi-photon absorption to be experimentally observed. We report the multi-photon absorption coefficients for $Ge_{23}Sb_7S_{70}$ within the measurement range corresponding to 3–11 photon absorption. The dispersive Kerr nonlinear index of the chalcogenide glass in the short-wave to mid-infrared wavelength range is measured, resulting in a peak n_2 value of 4.4×10^{-18} m^2/W. Enhancements to the nonlinear refractive index from the presence of defect states are observed. We further report experimentally verified multi-photon absorption excitation of photoluminescence in $Ge_{23}Sb_7S_{70}$ chalcogenide glasses. The results pave the way for previously unexplored, new paradigms of photonic device design leveraging very high order multi-photon absorption effects and multi-photon excited photoluminescence.

I. INTRODUCTION

Nonlinear optical processes are fundamental to a wide variety of applications including soliton formation for long haul data transmission, correlated photon pair generation for quantum communications and computing, and frequency combs enabling precision metrology and advanced light sources. While these applications rely solely on the real part of the nonlinear susceptibility; at the same time, efficient performance requires an imaginary nonlinear susceptibility that is as small as possible. Consequently, a commonly used metric to gauge the desirability of a material for nonlinear optical applications is the nonlinear figure of merit, which takes into account the real and imaginary parts of the nonlinear susceptibility, and the operating wavelength.

Despite the implications inherent in the nonlinear figure of merit, it is certainly not the case that the real part of the nonlinear susceptibility is the only element worth harnessing for sophisticated applications. A plethora of applications may in fact leverage

the imaginary part of the nonlinear susceptibility. These include photodetection,[1,2] pulse shaping through saturable absorption,[3,4] emerging 3D nanofabrication techniques,[5] optical pulse metrology,[6] and fluorescence spectroscopy.[7] Bio-imaging applications, in particular, are beneficiaries of high-order photon absorption (PA). In these processes, N photons incident on a material are absorbed, with the probability of the absorptive process occurring diminishing, as the photon order N is increased. The higher the order of multi-photon absorption (MPA) effects, the better the ability to utilize these effects in imaging applications: First, by virtue of higher order PA effects occurring at longer wavelengths, the potential for higher penetration depths and lower optical damage in non-destructive, *in vivo* imaging for biomedical applications is enhanced. Second, higher order nonlinear effects have better spatial confinement and therefore enable better resolution to be achieved in applications such as photodynamic therapy,[8] optical limiting,[9] bio-targeting,[10] and bio-sensing.[11] Consequently, the ability to quantify high order MPA coefficients is an important capability.
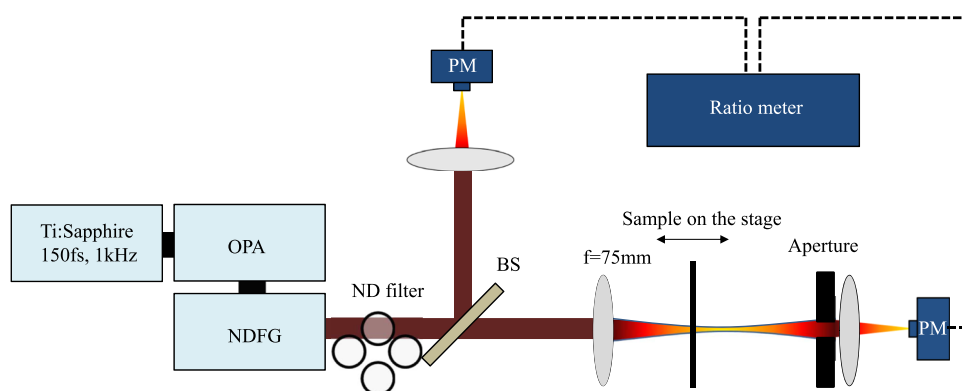
FIG. 1. Schematic of the z-scan setup for the measuring nonlinear coefficients in the range from near IR to far IR. OPA denotes the optical parametric amplifier, NDFG is a non-collinear difference frequency generator, and PM is an optical power meter.

The ability to design for and advantageously leverage the nonlinear optical properties of a material relies fundamentally on being able to quantify them. The quantification of high order nonlinear absorptive effects is challenging because of the difficulty in achieving the requisite optical intensities for observing high-order nonlinear absorption or similarly because optical changes from high order effects intended to quantify them are too small to detect with most tools. In addition, very high order MPA typically occurs at long wavelengths and requires materials which are optically transparent at these wavelengths to be successfully observed.

In this manuscript, we report the experimental measurement of MPA coefficients up to the eleventh order in $Ge_{23}Sb_7S_{70}$ (GSS) chalcogenide glass (ChG), by far the highest order MPA experimentally recorded to date. Open aperture z-scan and closed aperture z-scan measurements enabled through a high sensitivity detection system allow very small changes in optical intensities to be quantified. The schematic z-scan setup is shown in Fig. 1. To achieve a high signal to noise ratio, we normalize the transmittance with a reference beam split from the measurement pulse. In addition, tens of measurements are averaged to reduce effects from laser fluctuations. Details of the method used to retrieve nonlinear coefficients from raw data are provided in Sec. III.

The nonlinear refractive index corresponding to the real part of third susceptibility is also quantified from the short-wave (1.1 μm) to mid-infrared (5.0 μm) wavelengths with enhancements in the nonlinearity reported from the presence of defect states. We also report the excitation of photoluminescence in GSS using 4-PA. Such MPA-induced photoluminescence could provide new avenues of light generation in indirect bandgap materials. Consequently, we document in this manuscript, the ability to characterize very high order MPA in GSS up to the 11th order and the generation of photoluminescence via MPA. These capabilities could avail new potential applications in high resolution, non-destructive imaging, medicine, and high performance metrology.

II. RESULTS

A. Material, optical theory, and synthesis of $Ge_{23}Sb_7S_{70}$ chalcogenide glasses

GSS is a ternary chalcogenide glass (ChG).[12,13] Originally studied for their remarkable electronic and photonic properties, and their ability to undergo structural and phase changes for applications such as non-volatile memory and[14] chalcogenide glasses are actively studied today for photonic applications as they can be readily processed in bulk, thin film (planar), and fiber form. They possess broad transparency windows that span the near infrared to 20 μm, and large optical nonlinearities two orders of magnitude larger than in silica.[15–18] Furthermore, chalcogenide glasses possess tunable physical properties such as bandgap energy, refractive index, transparency window, nonlinear refractive index, and most recently tunable dispersion[19–21] realized through compositional alloying and microstructural engineering. The ability to tune these parameters is achieved through compositional engineering of their elemental constituents, Ge, P, Ga, As, and Sb, and chalcogen components, S, Se, and Te. This unique combination of structural stability, property tailoring, and compatibility with fabrication methods to realize low loss planar structures enables manufacturing of robust, monolithic photonic devices. Amongst the plethora of chalcogenide compounds available. GSS has important advantages over some other ChGs including resistance to oxidation[13] and being relatively inert to humidity[22] especially when compared to As–S, As–Se, and Ge–S glasses.

During glass production, carriers are generated. The glass is amorphous in nature, and carriers are not free. Rather, they are trapped in localized areas of disorder such as defects. The generated carriers are further associated with structural deformation induced by strong electric-phonon interactions. If the electric-phonon interactions are sufficiently strong and long in duration, the structure will be deformed. The localized states give rise to band tail states. The associated band tail energy behaves similarly to exciton states, in which they are not free but localized at structural defects. The quenched glass can exist in metastable states that may or may not be in equilibrium depending on production conditions and histories. Furthermore, dangling states can arise as a result of mid-gap energy states during quenched glass production. These mid-gap states can have effects on the optical and electrical properties of the amorphous glass.

The network units of the GSS glass consist of $SbS_{3/2}$ and $GeS_{4/2}$ structural units which dominate the backbone of the glass network.[12] If the glass network constituents possess variations in valency, coordination defects (such as electron or hole centers) can arise. The coordinated distance and angle between the network units are formed such that they possess minimum energy at zero temperature. Consequently, the network units are randomly connected.

The parameter means coordination number (MCN) defines the total number of valencies divided by the total number of atoms and is used to describe the glass states. It was previously documented that an MCN value of 2.4 and 2.67 gave rise to phase transitions[23,24] in some ChGs, which in turn can enable tunable device behavior for unique applications. The MCN for this GSS glass is 2.53, corresponding to an over-constrained, stressed-rigid glass. The over-constrained GSS is prone to having coordinated defects, which are bonding states that deviate from a fully coordinated network. The coordinated defects have mid-gap energy levels. The coordination defects that form during glass production can be annihilated. Conversely, it has also been shown and quantified that photo-induced coordination defects can be created, by mechanisms dependent on glass composition and the characteristics of the exciting radiation.[25,26] These phenomena could provide a lever for controlling the creation/modification of bonds and, thereby, allow relaxed amorphous structures to be controllably formed.[27,28] These defects impact a variety of optical properties, including the nonlinear optical behavior of the GSS material of interest in the present study. Material growth details of the $Ge_{23}Sb_7S_{70}$ used in this study are provided in Sec. III.

The intricacies of the GSS glass network formation is likely to give rise to a wealth of unique nonlinear optical properties, and understanding these intricacies is instrumental to the study of very high order nonlinear absorption processes and associated photoluminescence generation. First, the aforementioned localized defect states could contribute to the enhancement of the Kerr nonlinear index since the tail states decrease the bandgap energy, and the nonlinear refractive index is related to E_g^{-4} for the same ratio of photon energy to bandgap, where E_g is the bandgap energy.[29,30]

Second, the presence of mid-gap states could enable the generation of photoluminescence using MPA, particularly at wavelengths that correspond with the energies of the states. Consequently, we document in this manuscript, the ability to characterize very high order MPA in GSS up to the 11th order and the generation of photoluminescence via MPA.

B. Experimental quantification of 11-photon absorption coefficient

In order to characterize very high order multi-photon effects, we formulated a z-scan setup which possesses a wide wavelength range of optical pulses and detection capabilities. In particular, the optical detection is engineered to have a high signal to noise ratio that has enabled us to successfully characterize very small changes in optical intensities that are expected in high order MPA effects. Full details pertaining to the z-scan measurement setup are provided in Sec. III. In Nth order MPA, N photons are absorbed with the transition rate of the MPA process scaling with I^N, where I is the intensity of the incident light and N is the number of photons involved. The transition rate is described by Fermi's golden rule, $R = 2\pi/\hbar |M_{if}|^2 \rho(E_f)\delta(E_f - \sum_n E_n - E_i)$, where the transition matrix M_{if} can be calculated from Feynman diagrams. N-PA in indirect bandgap semiconductors has N vertex. Each vertex is proportional to $\sqrt{I}$ from the dipole interaction. The transition rate is proportional to I^N. The contributed number of photons is increased with wavelength according to the relation, $N \geq E_g/h\nu$, where N is the lowest integer meeting the inequality, E_g is a bandgap energy, and $h\nu$ is the photon energy. Because of the relatively large bandgap of GSS, very high order PA effects can be accessed at mid-infrared wavelengths.

The open z-scan experiments were performed at wavelengths between 1.6 μm and 6 μm. Higher order nonlinear absorption coefficients are measured up to 11PA, but 12PA corresponding range of wavelength 5.6 μm–6 μm is not measured since the variation of transmittance in open aperture z-scan is in the level of detection error. The measured nonlinear absorption coefficients extracted between 1.1 μm and 5.5 μm are shown in Fig. 2(a). The wavelength range corresponds to 3PA-11PA [plotted using scaled units as represented in the caption of Fig. 2(b)]. In Fig. 2(b), we plot the absorption per unit length as given by $\alpha_N I^{N-1}$, where N is the MPA order, α_N is the Nth order MPA coefficient, and I is the peak intensity. At low intensity, lower order MPA is stronger than higher order MPA. But, the absorption by higher order MPA effects increases faster relative to the lower orders as the peak intensity increases. For example, 6PA is lower than 10PA at lower peak intensities lower than 25 GW/cm^2, but 10PA has stronger absorption than 6PA at intensities exceeding 25 GW/cm^2.

The open z-scan measurements corresponding to the wavelengths where 4PA–12PA occur are shown in Fig. 3, where the characteristic dip is easily resolved for measurement wavelengths corresponding to MPA effects from 4PA–11PA. In the measurement region between 5.6 μm and 6 μm corresponding to 12PA, the open
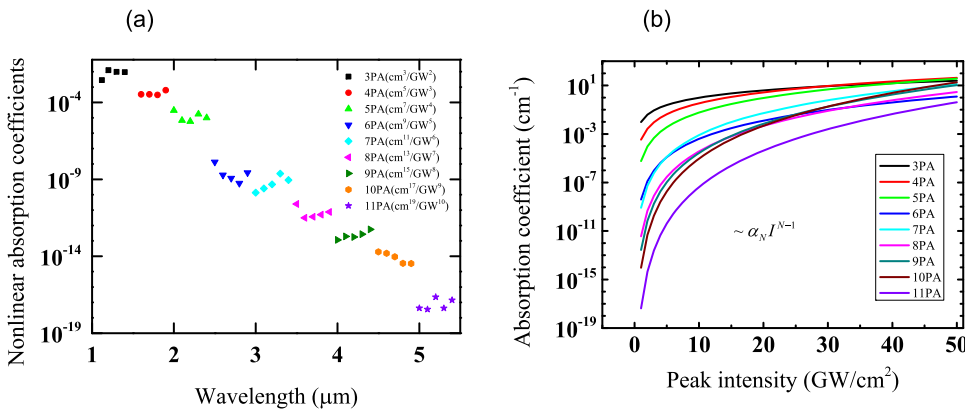
FIG. 2. (a) MPA coefficients, N-PA in the range of 1.1–5.5 μm in $Ge_{23}Sb_7S_{70}$ glass, where N denotes the number of contributed photons in the nonlinear absorption. The units of nonlinear absorption coefficients are shown in the figure legend. Errors bars for the nonlinear absorption coefficients are less than size of points. (b) Absorption vs. peak intensity of the MPA coefficients over the input peak intensity according to $\alpha_N I^{N-1}$.

FIG. 3. The measured open z-scan plots (black dots) and fits to the theoretical open z-scan function (red lines) at 4PA–12PA. The open z-scan plots were measured at a peak intensity not exceeding 50 GW/cm^2.

aperture z-scan dip could not be experimentally observed even at a high peak optical intensity of 50 GW/cm^2. The optical intensity used was intentionally limited to <50 GW/cm^2, in order to avoid laser-induced plasma breakdown and photo-induced structural changes in the sample.
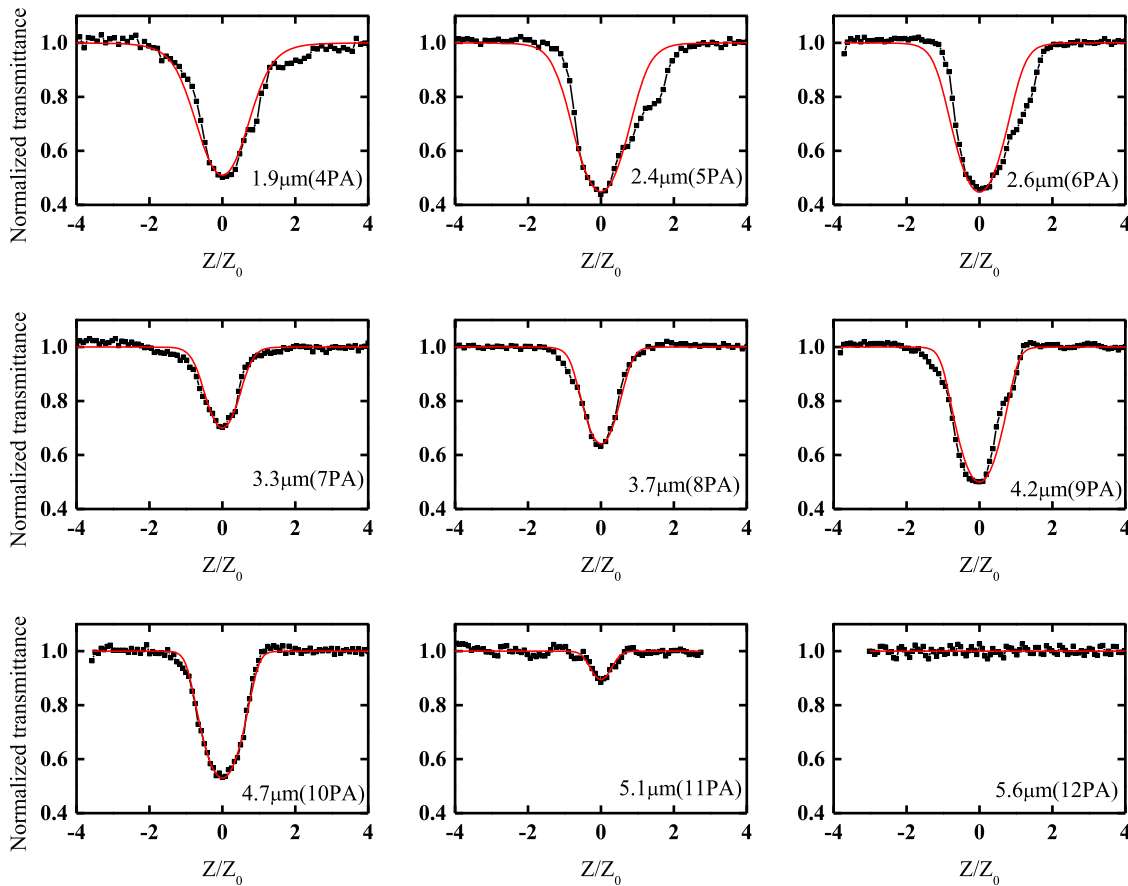
Three nonlinear optical effects other than that arising from the GSS′ Kerr nonlinearity may also contribute to the effects observed in z-scan measurements. These include thermal, free carrier, and saturable absorption effects. In our measurements, the thermal effect is expected to be negligible because the 150 fs temporal pulse width of the laser is too fast for thermal nonlinearities to manifest, especially when compared to the electron-phonon coupling time scale of ~1 ps. Furthermore, the heat generated dissipates with a time scale on the order of $\sim D^2/4\alpha$, where D is the laser spot size and α is the thermal diffusion coefficient. The GSS glass used in the experiments has a dissipation time scale of 40 μs, which is smaller than the 1 ms interval between pulses arriving on the substrate (laser's pulse repetition rate is 1 kHz). Thus, any generated heat will dissipate before the next pulse arrives thus precluding any possibility of thermal buildup. The electrons excited by MPA may give rise to saturation absorption and free carrier effects. These effects can be described by the

expressions, $\frac{d\Delta\phi}{dz'} = k(\gamma I + \sigma\Upsilon)$ and $\frac{dI}{dz'} = -(\alpha_0 I + \frac{\alpha_N}{1+I/I_s}I^N)$, where $\Delta\phi$ is the nonlinear phase distortion, z' is the coordinate in the propagation direction of the beam, k is the wave vector of the beam, γ is the Kerr nonlinear refractive index, σ denotes the change in refractive index induced by free carriers, N is the number of photons induced in the MPA, and I_s is the saturation intensity. The free carriers excited by MPA are described by $\Upsilon = \int_{-\infty}^{t} \frac{\alpha_N I^N(t')}{N\hbar\omega}dt'$. The free carrier term has an effect only on closed aperture z-scan measurements, whereas the saturation absorption term has an effect only on open z-scan measurements. The nonlinear absorption saturation term can be expanded according to a Taylor series of I/I_s, $\alpha_N/(1 + I/I_s)I^N = \alpha_N I^N + \alpha_N I^{N+1}/I_s + \cdots$. The nonlinear absorption saturation effect can be characterized by investigating the nonlinear absorption coefficient as a function of input intensity of light. The measured nonlinear absorption coefficient will be a function of laser intensity. The dependency was less than 10% in the GSS material within 50G W/cm^2 peak intensity. The nonlinear absorption saturation effect could be ignored in this paper. Therefore, we conclude that the dip observed in the open z-scan measurements is dominated by nonlinear absorption induced by multi-photon transitions from the valence band toward the conduction band.

C. Experimental observation of photoluminescence excited by multi-photon absorption

Electrons and holes excited by MPA can be relaxed via phonon-electron interactions to smaller energy states (such as states within the band) before recombination. In this case, photoluminescence at wavelengths much longer than that corresponding to the bandgap energy is possible. The existence of photoluminescence is further evidence that the absorption dip observed in open z-scan measurements is induced from MPA. Furthermore, observations of photoluminescence at longer wavelengths also provide information about bandgap states created by defects. The measured photoluminescence spectrum can also provide information about localized mid-gap states, any influence from Urbach tails and shed light on how they relate to the GSS glass formation process and the material's resulting structural arrangement.

We experimentally characterize photoluminescence of GSS at the wavelength range between 0.6 μm and 1.7 μm using an excitation pump located at 2 μm. Full details of the photoluminescence characterization method are provided in Sec. III. Figure 4(a) shows the measured photoluminescence as the input laser intensity is varied. The photoluminescence signal is observed to exist at the wavelength range between 900 nm and 1700 nm, corresponding to an energy of ~$0.32E_g$–$0.54E_g$ where E_g for GSS was previously shown to be 2.5 eV.[31] The 3 dB bandwidth of the photoluminescence excited by the 2 μm pump spans from 1.27 μm to 1.7 μm and covers the complete O to L telecommunication bands. The broad continuum of wavelengths where photoluminescence is observed is expected from GSS's amorphous nature. We postulate that the presence of photoluminescence in this wavelength range is due to the presence of localized mid-gap states. Early studies

pertaining to luminescence in amorphous semiconductors[32] suggests that the redshifted photoluminescence observed in Fig. 4(a) is consistent with GSS being an amorphous material with charged dangling states. The photo-induced electrons and holes are first trapped by charged defects, before subsequently going through radiative recombination and generating the PL signal in the process. FTIR data of the GSS glass are used to extract the Urbach energy from the fitting equation, $\log \alpha = \log \alpha_0 + (hv - hv_0)/E_u$, where α denotes the linear absorption coefficient, hv is the photon energy, and E_u is the Urbach energy. As shown in Fig. 4(d), the Urbach energy is extracted to be 0.13 eV, a value that is too small to account for the photoluminescence observed in Fig. 4(a). It is therefore likely that the observed photoluminescence is attributed to the presence of localized mid-gap states, corresponding to a transition energy difference ~$0.32E_g$–$0.54E_g$. The presence of localized states is also known to alter the recombination lifetime between electrons and holes.[33] The recombination lifetime is shorter in localized mid-gap states than in localized band edge states. This implies that the localized mid-gap states enhance the recombination process over band edge states. Figure 4(c) shows the locations and magnitudes of the energies associated with the GSS film, as extracted using the photoluminescence measurements.

For an Nth order MPA process, the generated photoluminescence intensity, P_{PL}, is proportional to the intensity of the input source according to the expression, $P_{PL} \propto I_{in}^N$, where N denotes the order of the MPA process, P_{PL} is the photoluminescence power, and I_{in} is the intensity of the input light source. The generated photoluminescence power is spectrally integrated and plotted as a function of input power [see Fig. 4(b)]. The slope of the plotted data corresponds to the contributed number of photons in the nonlinear
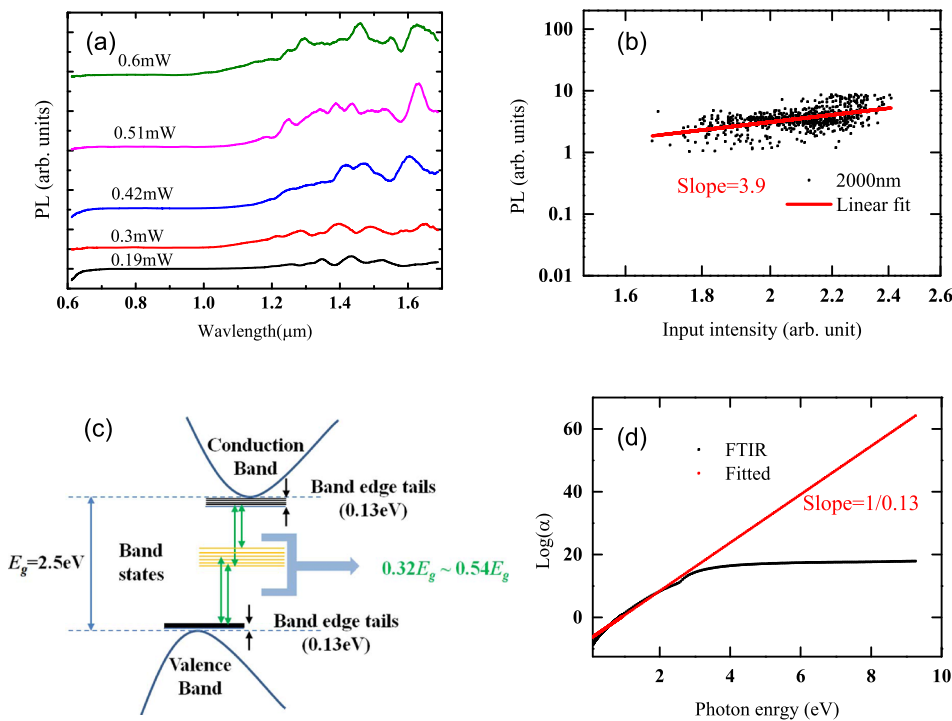
FIG. 4. Photoluminescence in GSS stimulated by 4-PA. The pump wavelength is fixed at 2000 nm. (a) Measured photoluminescence of the GSS as the input laser power is varied. (b) Integrated photoluminescence power as a function of laser input power showing the 4th order power law relationship (c) Energy band diagram illustrating the locations and magnitudes of the energies associated with the GSS film, as extracted using the photoluminescence measurements. (d) The Urbach energy of GSS is extracted using FTIR to be 0.13 eV.

absorption process. The value of the slope is extracted to be 3.9, which is very close in value to the whole integer 4. This implies that 4-PA is the dominant effect here. Furthermore, the energy bandgap of GSS previously characterized to be ~2.5 eV implies that at a pump wavelength between 1.98 μm and 2.48 μm, 4-PA should be in effect. Therefore, the results obtained from photoluminescence characterization are in good agreement.

Multi-photon excited photoluminescence of target molecules has been used not only for their advantageous nonlinear properties but to avoid structure deformation from strong linear absorption in photosensitive amorphous glass systems. Well known examples of photo-induced changes to chalcogenide glasses include photo-diffusion,[34] photo-fluidity,[35] and photo-crystallization.[36] In particular, photo-crystallization is a process which results in an irreversible structural change. Photo-induced structural deformation can be minimized to maintain desired optical properties and performance, with knowledge of MPA in the pumping process. Such knowledge is critical in applications where high pump intensities are required, such as supercontinuum or high harmonic generation.

D. Nonlinear refractive index enhancement from defect states

Next, we characterize the Kerr nonlinearity of GSS in the short-wave to mid-infrared wavelength range, spanning from 1.1 μm to 5.0 μm. Details pertaining to the characterization of the Kerr nonlinearity are provided in Sec. III. The Kerr nonlinear refractive index,

n_2, quantifies the nonlinear optical phase modulation occurring in a material and is a fundamental quantity needed for the design of all-optical devices leveraging the third order nonlinear susceptibility. The measured values are shown in Fig. 5. We measure a peak n_2 value of 4.4×10^{-18} m^2/W, located at a wavelength of 1.2 μm. The peak wavelength is located close to the 2-PA edge, in line with theoretical predictions from Kramers-Krönig relations between the 2-PA coefficient and the nonlinear refractive index, $n_2(\omega) = \frac{c}{\pi} \int_0^\infty \frac{\beta_{TPA}(\omega,\omega')}{\omega'^2 - \omega^2} d\omega'$.[37] The location of the n_2 peak is slightly redshifted from the two-photon absorption (TPA) edge of 1.13 μm defined with the absorption coefficient of 10^2 cm^{-1}. We postulate that this red-shift is attributed to localized states which arise from the presence of defects. The band edge is not sharp, owing to the presence of defects and the amorphous nature of the GSS glass.

Kramers-Krönig relations predict a peak n_2 value at the two-photon edge, followed by a monotonic decrease and plateauing of n_2 at longer wavelengths. However, we observe from Fig. 5(d) the presence of n_2 resonance peaks at wavelengths, 1.9 μm (0.65 eV), 2.4 μm (0.52 eV), 3.2 μm (0.39 eV), and 4.5 μm (0.28 eV), located at the number labels from (2)–(5). The observed enhancements in n_2 are postulated to be due to MPA effects in the presence of band states. Figure 5(e) illustrates the possible transitions in the presence of band states. Label (1) denotes the wavelength where the 2-PA edge is located, between valence band and conduction band. Labels (2) and (3) denote 2-PA between the valence-band states and the band
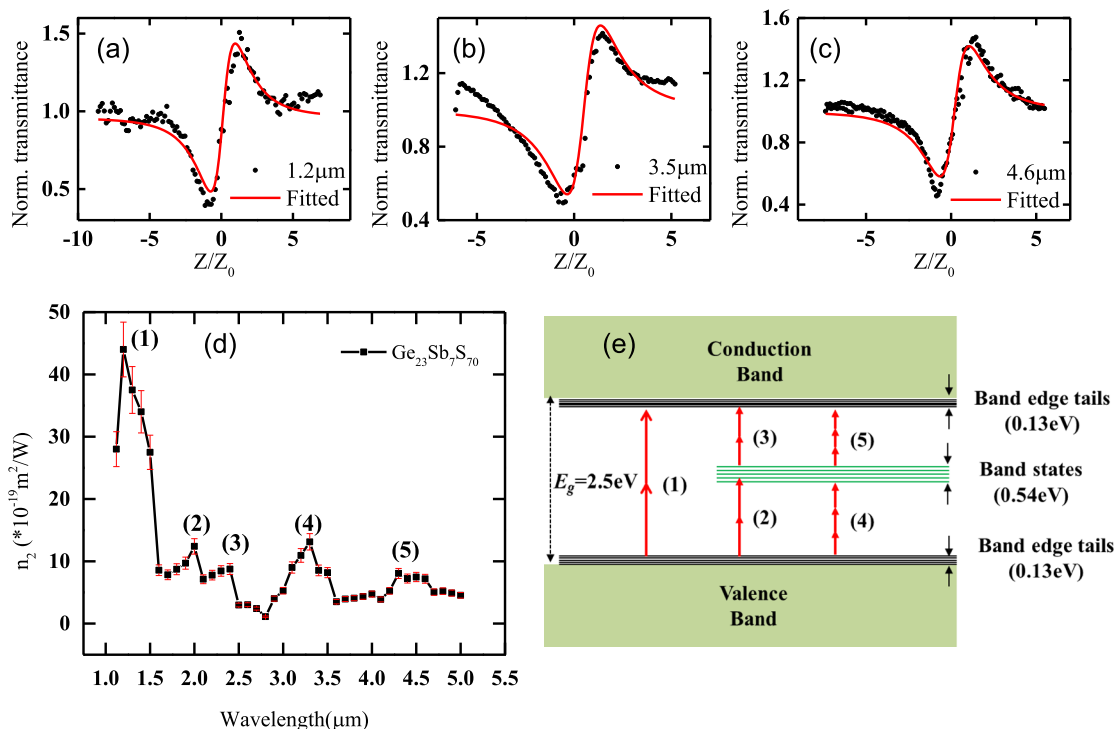
FIG. 5. Characterization of the nonlinear refractive index of Ge$_{23}$Sb$_7$S$_{70}$ glass using closed aperture z-scan measurements. Measured closed aperture z-scan profiles of GSS at wavelengths of (a) 1.2 μm, (b) 3.5 μm, and (c) 4.6 μm. (d) Measured Kerr nonlinear refractive index of GSS from 1.1 μm to 5.0 μm, where the red bars denote 10% error bars in the measurement. (e) Schematic diagram for the role of band states on enhanced nonlinear refractive index.

states, as well as that between the band states and the conduction band states. The two-absorption resonance is related to the n_2 enhancement predicted by the Kramers-Krönig relation. The nonlinear refractive index enhancement in (4) and (5) occurs as a result of higher order nonlinear effects, namely, the fifth-order nonlinear susceptibility, $\chi_{(5)}(\omega; \omega, -\omega, \omega, -\omega, \omega)$. The fifth order nonlinear susceptibility contributes to a higher order nonlinear refractive index, n_4, and generates a change in refractive index, Δn, according to the equation, $\Delta n = n_4 I^2$. The Kramers-Krönig relation pertaining to n_4 and 3-PA can be inferred as $n_4(\omega) = \frac{c}{\pi} \int_0^\infty \frac{\beta_3(\omega, \omega, \omega')}{\omega'^2 - \omega^2} d\omega'$, where β_3 is the 3-PA coefficient. n_4 possesses the highest value at the three-photon resonance edge. The width of the band states can be obtained as 0.54 eV, from the measured PL in Fig. 4(a), ~$0.32E_g$–$0.54E_g$. The PL broadening is from mainly the broaden band states since the electron and hole reach edge states after faster recoil dynamics of the carriers by phonons than the radiational recombination. The position of band states in the energy diagram can be extrapolated from the location of n_2 resonant peaks. This may be done by using the expression $x + y + E_b = E_g$, where x denotes the energy difference between the valence band and band states, y is the difference between the conduction band and band states, $E_b = 0.3$ eV is the estimated shift in the band edge from the Urbach energy, and $E_g = 2.5$ eV is the bandgap energy. We note further that this is an estimated value because the exact density of states in the bands is unknown. We postulate further that the resonant two photon absorption at 1.9 μm (0.65 eV) and 2.4 μm (0.52 eV) and the resonant three photon absorption at 3.2 μm (0.39 eV) and 4.5 μm (0.28 eV) could be used to obtain the following equations, $x \sim 2 \times 0.65$ eV $\sim 3 \times 0.39$ eV and $y \sim 2 \times 0.52$ eV $\sim 3 \times 0.28$ eV. Consequently, we derive approximate values of x and y as ~1.2 eV and ~1 eV, respectively. The gap energy between valence band and band states of 1.2 eV and the gap energy between the conduction band and band states of 1 eV agree relatively well and provide a good explanation as to the cause of the observed resonant peaks in n_2.

As predicted by Kramers-Krönig relations that govern n_2 and the two-photon absorption coefficient, in the absence of band states, the n_2 value should plateau at wavelengths beyond 2.5 μm. The n_2 value for GeSbS at the plateaued region can be estimated as 4×10^{-19} m^2/W at 3.8 μm or 5 μm (wavelengths far from the TPA or 3PA resonance regions). The n_2 value at 3.3 μm is 10×10^{-19} m^2/W. Consequently, it means that there is a resonant enhancement in the n_2 value from 4×10^{-19} m^2/W to 10×10^{-19} m^2/W as a result of existing band states.

III. METHODS

A. Ge$_{23}$Sb$_7$S$_{70}$ material growth

Bulk chalcogenide glasses of GSS were prepared by a conventional melt-quenching technique. All glasses were prepared using high purity raw materials (metals basis) from Alfa-Aesar: Ge (99·999%), Sb (99·999%), and S (99·999%). These elements were carefully weighed and batched in a nitrogen purged MBraun Labmaster 130 glove box. The weighed batches were loaded into cleaned fused quartz tubes and sealed under vacuum using a methane-oxygen torch to form sealed ampoules. The batches were melted in a rocking furnace overnight at a melting temperature, $T_m = 850$ °C. After overnight rocking at elevated temperature, the furnace was

then cooled to the quench temperature, $T_Q = 800$ °C, prior to removal from the furnace for quenching which was performed by natural convection in air using compressed air flowing over the ampoule. To minimize the quench-related stress, glasses were annealed at 270 °C for 2 h and cooled to room temperature. The prepared glass rods were removed from the ampoules and cut and grinded into multiple specimens with a dimension of 6 mm × 6 mm × 2 mm using a slow speed saw and a silicon carbide grinding paper with fine grit sizes, respectively. The specimens were subsequently polished on both sides using a polishing pad with 0.05 μm Al$_2$O$_3$ slurry.

B. Nonlinear characterization

The z-scan method is used to characterize nonlinear optical properties of the GSS material. The laser beam is focused by a CaF$_2$ lens with a focal length of 75 mm, and the sample is scanned in the z-direction. The induced nonlinear phase from the sample changes the transverse light intensity on the far field screen. An aperture is used to measure the changed transverse distribution of the intensity. Open aperture z-scans allow us to extract information on the multi-photon absorption. The multi-photon absorption coefficients were extracted by performing a numerical fit to the expression, $T_{nPA} = 1/\{1 + (N - 1)\alpha_N L_{eff}^{(N)}[I_{00}/(1 + (z/z_0)^2)]^{N-1}\}^{1/(N-1)}$, where N is the contributed number of photons, α_N refers to the absorption coefficients, I_{00} is the peak intensity of the beam at the focal point, z_0 is the Rayleigh length, and $L_{eff}^{(N)}$ is the effective thickness of the sample. Closed aperture z-scan measurements are used to obtain the nonlinear refractive index. We exploited 40% transmittance of the aperture to extract the nonlinear refractive index by fitting the function, $T = 1 + \frac{4\Delta\phi z/z_0}{[1+(z/z_0)^2][9+(z/z_0)^2]}$, where $\Delta\phi = 2\pi I_{00} L_{eff} \, n_2/\lambda$ is the nonlinear phase. Optical pulses with a temporal duration of 150 fs with 1 kHz repetition rate in the wavelength range from 1.6 μm to 6 μm are generated using optical parametric amplification and difference frequency generation from a Ti:Sapphire laser pump. A peak power less than 50 GW/cm^2 at the focal point is used to avoid laser damage of the GSS sample. The calculated Rayleigh length for the z-scan setup is between 3.1 mm and 9.4 mm. The GSS sample is 2 mm thick and therefore smaller than the Rayleigh length and satisfies the thin sample condition. The main cause of noise in the z-scan method is from the laser power fluctuation. To maximize the signal to noise ratio, the laser is split using a 50:50 CaF$_2$ beam splitter to create a reference beam. The transmitted optical power may then be normalized by the reference beam such that laser fluctuation effects are reduced by 90%. Additional noise reduction is achieved by averaging of the measurements. The approach we used allows very small intensity changes in the open aperture z-scan measurements to be detected.

C. Photoluminescence characterization

To measure the photoluminescence of the sample, a Mid-IR pump beam with a wavelength of 2 μm corresponding to 4-PA is used. The pump beam has a spectral bandwidth of 50 nm and a temporal width of 150 fs. The optical line filter having optical density (OD) larger than 5.5 is used to eliminate spontaneous radiation from the laser source that contributes to unwanted noise. The luminescence is collected by a reflective collimator. To minimize an

unwanted collection of the pump beam, the reflective collimator is marginally tilted from the pump beam direction and a short pass filter with OD larger than 6 is used to minimize unwanted collection of the pump beam. An optical spectrum analyzer with high resolution and a very low noise floor level of −100 dBm in the scanning spectral range of 0.6 μm–1.7 μm is used to analyze the spectrum of the 4-PA excited photoluminescence.

IV. DISCUSSION

We have previously characterized the nonlinear refractive index of GSS in a planar form. At the 1.55 μm wavelength, the nonlinear refractive index characterized via self-phase modulation experiments in GSS waveguides was 3.71×10^{-18} m^2/W, which is similar to the value of 2.0×10^{-18} m^2/W measured here using bulk GSS samples. It has been documented previously that certain classes of chalcogenide glasses possess different nonlinear behavior in bulk form versus film form for some ChGs. As noted in Refs. 38 and 39, binary or simple isostructurally similar (S–Se) ternary glasses containing 3-coordinated (As) and 2-coordinated (S/Se) species can show significant variations in their bond arrangements (angle and lengths) between the bulk and film states. Additionally, the energetics of such deposition techniques can also enhance how far away the resulting film is from the lower energy, (near-) equilibrium configuration observed in bulk glasses.[12] Such structural variation is due to the presence of isostructural, 2-coordinated S, and Se, which impacts the layer-like characteristic in As–S–Se glasses. The lower MCN of such glasses imparts a degree of flexibility to the structure to rearrange during the deposition process. This creates a greater potential variation in the glass structure and properties. Ge–Sb–S has a higher MCN and rigidity and thus possesses less variation in network confirmation between its bulk and thin film forms. For this reason, one expects less variability in how the structural units arrange themselves during deposition, resulting in a smaller variation in the bulk/film property.

The high order multi-photon absorption demonstrated in this manuscript may be useful for bio-imaging applications. Higher penetration depths, low *in situ* damage, and greater spatial confinement availed through very high order multi-photon absorption may be advantageously leveraged for improvements in bio-imaging systems. To facilitate imaging of biological specimens or nanostructures, GSS may be utilized as labels of biomaterials, particularly in nanostructured forms such as GSS quantum dots or nanoparticles.

To date, observations of MPA-induced stimulated emission have been limited largely to solution-based chemicals. 3- and 5-PA excited stimulated emissions have been reported in (4-[N-(2-hydroxyethyl)-N_-(methyl)amino phenyl]-4'-(6-hydroxyhexyl sulphonyl) stilbene) chromophores[40,41] and fluorophores respectively.[42] Gold nano-antennas were also reported to exhibit four-photon induced photoluminescence. The demonstrated excitation of fluorescence using 4-PA in GeSbS avails the ability to cast the material into planar, nano-structured devices that could be leveraged for photonic integrated circuits, beyond the form availed by purely solution-based chemicals. Of note, the 4-photon observed photoluminescence possesses a 3 dB bandwidth from 1.27 μm to 1.7 μm and covers the complete O– to L–telecommunications bands.

Furthermore, the ability to quantify very high order MPA coefficients of up to the eleventh order is an unprecedented capability

and provides the fundamental quantities needed for the design of systems leveraging high-order PA effects. Knowledge of MPA coefficients is instrumental to estimating the probability of multi-photon transitions occurring and therefore provides quantitative information regarding the number of photons or incident optical intensity required for a specific system.[42,43] The demonstration of very high order MPA up to the 11th order brings us a step closer toward the design of optical systems that leverage the unparalleled resolution and dynamic range availed by high-order multi-photon transitions.

V. CONCLUSION

Very high order MPA coefficients of GSS were measured up to the 11PA coefficient. The ability to quantify very high order MPA coefficients was enabled by a high sensitivity detection system in the z-scan setup. The dispersive Kerr nonlinear refractive index of GSS in the mid-IR range was also measured and exhibits its peak value near the 2-PA edge, in line with Kramers-Krönig relations between Kerr nonlinear index and 2-PA. Enhanced n_2 values were experimentally observed at wavelengths corresponding to two- and three-photon resonances between extended states and midgap states. The nonlinear refractive index enhancement by existing defect states is an important result that shows that nonlinear optical properties of materials can be tailored by careful control of defects. Photoluminescence measurements provided evidence of mid-gap states in the GSS material, corresponding to a transition energy difference $\sim 0.32 E_g$–$0.54 E_g$. It was further shown that photoluminescence in the GSS film could be stimulated with 4-PA, a feature that could bring about significant new pathways for light generation in planar photonic nano-devices. The observation of photoluminescence at wavelengths much longer than usual is an outstanding result, as it provides critical information on localized bandgap states generated by valence defects.

The reported results are significant for future development of photonic systems leveraging very high order MPA such as high resolution, non-invasive imaging, biomedicine, and precision metrology.

REFERENCES

[1] R. Hayakawa, N. Ishikura, H. C. Nguyen, and T. Baba, Appl. Phys. Lett. **102**, 031114 (2013).
[2] T. K. Liang and H. K. Tsang, Appl. Phys. Lett. **81**, 1323 (2002).
[3] Q. Bao, H. Zhang, Z. Ni, Y. Wang, L. Polavarapu, Z. Shen, Q.-H. Xu, D. Tang, and K. P. Loh, Nano Res. **4**(3), 297–307 (2011).
[4] M. Jiang, Y. Kumamoto, A. Ishii, M. Yoshida, T. Shimada, and Y. K. Kato, Nat. Commun. **6**, 6335 (2015).

[5] Y. L. Zhang, Q. D. Chen, H. Xia, and H. B. Sun, Nano Today **5**(5), 435–448 (2010).

[6] J. I. Dadap, G. B. Focht, D. H. Reitze, and M. C. Downer, Opt. Lett. **16**, 499–501 (1991).

[7] N. S. Makarov, J. Campo, J. M. Hales, and J. W. Perry, Opt. Mater. Express **1**, 551–563 (2011).

[8] A. V. Kachynski, A. Pliss, A. N. Kuzmin, T. Y. Ohulchanskyy, A. Baev, J. Qu, and P. N. Prasad, Nat. Photon **8**, 455–461 (2014).

[9] J. E. Ehrlich, X. L. Wu, I.-Y. Lee, Z.-Y. Hu, H. Rockel, S. R. Marder, and J. W. Perry, Opt. Lett. **22**, 1843–1845 (1997).

[10] X. Michalet, F. F. Pinaud, L. A. Bentolila, J. M. Tsay, S. Doose, J. J. Li, G. Sundaresan, A. M. Wu, S. S. Gambhir, and S. Weiss, Science **307**, 538–544 (2005).

[11] S. J. Pond, O. Tsutsumi, M. Rumi, O. Kwon, E. Zojer, J.-L. Bredas, S. R. Marder, and J. W. Perry, J. Am. Chem. Soc. **126**, 9291–9306 (2004).

[12] J. D. Musgraves, N. Carlie, J. Hu, L. Petit, A. Agarwal, L. C. Kimerling, and K. A. Richardson, Acta Mater. **59**(12), 5032–5039 (2011).

[13] Q. Du, Y. Huang, J. Li, D. Kita, J. Michon, H. Lin, L. Li, S. Novak, K. Richardson, W. Zhang, and J. Hu, Opt. Lett. **41**(13), 3090–3093 (2016).

[14] S. Hudgens and B. Johnson, MRS Bull. **29**(11), 829–832 (2004).

[15] K. A. Richardson, J. M. McKinley, B. Lawrence, S. Joshi, and A. Villeneuve, Opt. Mater. **10**, 155–159 (1998).

[16] K. A. Richardson, T. Cardinal, H. Shim, G. Stegeman, A. Schulte, R. Beathy, K. LeFoulgoc, C. Meneghini, J. F. Viens, and A. Villeneuve, J. Non-Cryst. Solids **256–257**, 353–360 (1999).

[17] E. C. Mägi, L. B. Fu, H. C. Nguyen, M. R. E. Lamont, D. I. Yeom, and B. J. Eggleton, Opt. Express **15**(16), 10324–10329 (2007).

[18] M. R. Lamont, C. M. de Sterke, and B. J. Eggleton, Opt. Express **15**(15), 9458–9463 (2007).

[19] M. Kang, L. Sisken, J. Cook, C. Blanco, M. Richardson, I. Mingareev, and K. Richardson, Opt. Mater. Express **8**, 2722–2733 (2018).

[20] L. Sisken, C. Smith, A. Buff, M. Kang, K. Chamma, P. Wachtel, J. D. Musgraves, R. Rivero-Baleine, A. Kirk, M. Kalinowski, M. Melvin, T. S. Mayer, and K. Richardson, Opt. Mater. Express **7**, 3077–3092 (2017).

[21] M. Kang, A. M. Swisher, A. V. Pogrebnyakov, L. Liu, A. Kirk, S. Aiken, L. Sisken, C. Lonergan, J. Cook, T. Malendevych, F. Kompan, I. Divliansky, L. B. Glebov, M. C. Richardson, C. Rivero-Baleine, C. G. Pantano, T. S. Mayer, and K. Richardson, Optics. Adv. Mater. **30**, 1803628 (2018).

[22] I. Watanabe, M. Ishikawa, and T. Shimizu, J. Phys. Soc. Jpn. **45**, 1603–1609 (1978).

[23] H. He and M. F. Thorpe, Phys. Rev. Lett. **54**, 2107–2110 (1985).

[24] M. F. Thorpe, J. Non-Cryst. Solids **57**, 355–370 (1983).

[25] S. Novak, V. Singh, C. Monmeyran, A. Ingram, Z. Han, N. Borodinov, N. Patel, Q. Du, J. Hu, I. Luzinov, R. Golovchak, A. Agarwal, and K. Richardson, J. Non-Cryst. Solids **455**, 29–34 (2016).

[26] J. D. Musgraves, K. Richardson, and H. Jain, Opt. Mater. Express **1**(5), 921–935 (2011).

[27] K. Shimakawa, A. Kolobov, and S. R. Elliott, Adv. Phys. **44**, 475–588 (1995).

[28] B. J. Eggleton, B. Luther-Davies, and K. Richardson, Nat. Photonics **5**, 141–148 (2011).

[29] H. Garcia and R. Kalyanaraman, J. Phys. B : At., Mol. Opt. Phys. **39**, 2737–2746 (2006).

[30] M. Sheik-Bahae, D. C. Hutchings, D. J. Hagan, and E. W. van Stryland, IEEE J. Quantum Electron. **27**, 1296–1309 (1991).

[31] J. W. Choi, Z. Han, B.-U. Sohn, G. F. R. Chen, C. Smith, L. C. Kimerling, K. A. Richardson, A. M. Agarwal, and D. T. H. Tan, Sci. Rep. **6**, 39234 (2016).

[32] R. A. Street, Adv. Phys. **25**(4), 397–453 (1976).

[33] W. Shockley and W. T. Read, Jr., Phys. Rev. **87**, 835–842 (1952).

[34] T. Wagner, J. Optoelectron. Adv. Mater. **4**, 717–727 (2002).

[35] P. Pradhan, R. Naik, N. Das, and A. K. Panda, Opt. Laser Technol. **96**, 158–165 (2017).

[36] K. Tanaka, A. Saitoh, and N. Terakado, J. Optoelectron. Adv. Mater. **8**, 2058–2065 (2006).

[37] B.-U. Sohn, C. Monmeyran, L. C. Kimerling, A. M. Agarwal, and D. T. H. Tan, Appl. Phys. Lett. **111**, 091902 (2017).

[38] L. Petit, A. Humeau, N. Carlie, G. Boudebs, H. Jain, A. Miller, and K. Richardson, Mater. Res. Bull. **42**, 2107–2116 (2007).

[39] L. Petit, N. Carlie, K. C. Richardson, M. Couzi, F. Adamietz, and V. Rodriguez, Mater. Chem. Phys. **97**, 64–70 (2006).

[40] G. S. He, P. P. Markowicz, T. C. Lin, and P. N. Prasad, Nature **415**, 767–770 (2002).

[41] Q. Zheng, H. Zhu, S. C. Chen, C. Tang, E. Ma, and X. Chen, Nat. Photonics **7**(3), 234–239 (2013).

[42] R. Carriles, D. N. Schafer, K. E. Sheetz, J. J. Field, R. Cisek, V. Barzda, A. W. Sylvester, and J. A. Squier, Rev. Sci. Instrum. **80**, 081101 (2009).

[43] C. D. Andrade, C. O. Yanez, H.-Y. Ahn, T. Urakami, M. V. Bondar, M. Komatsu, and K. D. Belfield, Bioconjugate Chem. **22**, 2060–2071 (2011).